The Plant Cell, Vol. 28: 2261–2275, September 2016, www.plantcell.org

Grana-Localized Proteins, RIQ1 and RIQ2, Affect the Organization of Light-Harvesting Complex II and Grana Stacking in Arabidopsis[OPEN]

Ryo Yokoyama,[a] Hiroshi Yamamoto,[a,b] Maki Kondo,[c,d] Satomi Takeda,[e] Kentaro Ifuku,[f] Yoichiro Fukao,[g] Yasuhiro Kamei,[d] Mikio Nishimura,[c] and Toshiharu Shikanai[a,b,1]

[a] Department of Botany, Graduate School of Science, Kyoto University, Sakyo-ku, Kyoto 606-8502, Japan
[b] Core Research for Evolutional Science and Technology (CREST), Japan Science and Technology Agency, Chiyoda-ku, Tokyo 102-0076, Japan
[c] Department of Cell Biology, National Institute for Basic Biology, Okazaki 444-8585, Japan
[d] Spectrography and Bioimaging Facility, National Institute for Basic Biology, Okazaki 444-8585, Japan
[e] Department of Biological Science, Graduate School of Science, Osaka Prefecture University, Sakai 599-8531, Japan
[f] Graduate School of Biostudies, Kyoto University, Sakyo-ku, Kyoto 606-8502 Japan
[g] Department of Bioinformatics, Ritsumeikan University, Kusatsu, Shiga 525-8577, Japan

Grana are stacked thylakoid membrane structures in land plants that contain PSII and light-harvesting complex II proteins (LHCIIs). We isolated two *Arabidopsis thaliana* mutants, *reduced induction of non-photochemical quenching1* (*riq1*) and *riq2*, in which stacking of grana was enhanced. The *curvature thylakoid 1a* (*curt1a*) mutant was previously shown to lack grana structure. In *riq1 curt1a*, the grana were enlarged with more stacking, and in *riq2 curt1a*, the thylakoids were abnormally stacked and aggregated. Despite having different phenotypes in thylakoid structure, *riq1*, *riq2*, and *curt1a* showed a similar defect in the level of nonphotochemical quenching of chlorophyll fluorescence (NPQ). In *riq curt1a* double mutants, NPQ induction was more severely affected than in either single mutant. In *riq* mutants, state transitions were inhibited and the PSII antennae were smaller than in wild-type plants. The *riq* defects did not affect NPQ induction in the chlorophyll *b*-less mutant. *RIQ1* and *RIQ2* are paralogous and encode uncharacterized grana thylakoid proteins, but despite the high level of identity of the sequence, the functions of RIQ1 and RIQ2 were not redundant. RIQ1 is required for RIQ2 accumulation, and the wild-type level of RIQ2 did not complement the NPQ and thylakoid phenotypes in *riq1*. We propose that RIQ proteins link the grana structure and organization of LHCIIs.

INTRODUCTION

In the chloroplasts of land plants, the PSII supercomplex consists of two PSII cores and associated light-harvesting complex II proteins (LHCIIs). This supercomplex is enriched in highly stacked thylakoid regions of appressed membranes known as grana (Dekker and Boekema, 2005). Light energy absorbed by LHCIIs is transferred to a special pair of chlorophyll molecules in the PSII reaction center to drive electron transport though downstream protein complexes in the thylakoid membrane. Under very high light intensities, excess absorbed light energy is dissipated as heat. This process can be monitored as the qE (energy-dependent quenching) component of the nonphotochemical quenching of chlorophyll fluorescence (NPQ). qE is induced by lumenal acidification, which depends on photosynthetic electron transport. A thylakoid-localized protein, PsbS, senses low lumen pH to induce qE (Li et al., 2000). Lumen acidification also activates violaxanthin deepoxidase, which catalyzes conversion of violaxanthin to zeaxanthin via antheraxanthin (xanthophyll cycle) (Niyogi et al., 1998).

As a result of these events, some LHCIIs detach from PSII, leading to aggregation of the disassociated LHCIIs around the PSII-LHCII supercomplex. This dynamic reorganization results in qE induction at both aggregated LHCIIs and still bound LHCIIs, which are referred as quenching sites Q1 and Q2, respectively (Holzwarth et al., 2009; Johnson et al., 2011, Minagawa, 2013). Besides qE, several additional components of NPQ have been proposed. qZ is a zeaxanthin-dependent component and is formed and relaxed with 10 to 15 min lifetime (Nilkens et al., 2010). qT is induced as a result of state transitions and qI is induced following PSII photoinhibition. State transitions balance the excitation pressure between PSII and PSI via relocation of LHCIIs (Kouřil et al., 2012). qI is associated with damage to the D1 protein, leading to photoinhibition and reduced photosynthetic capacity (Aro et al., 1993). The impaired PSII reaction center is able to quench fluorescence directly (Horton et al., 1996), but the exact mechanism is still unknown. Although qZ, qT, and qI components are slowly induced and relaxed (several minutes to hours), the kinetics of qE induction and relaxation are so fast (several seconds to minutes) that plants can respond to rapid fluctuations in light conditions

[1] Address correspondence to shikanai@pmg.bot.kyoto-u.ac.jp.
The author responsible for distribution of materials integral to the findings presented in this article in accordance with the policy described in the Instructions for Authors (www.plantcell.org) is: Toshiharu Shikanai (shikanai@pmg.bot.kyoto-u.ac.jp).
[OPEN]Articles can be viewed without a subscription.
www.plantcell.org/cgi/doi/10.1105/tpc.16.00296

(Li et al., 2009; Jahns and Holzwarth, 2012). Recently, a qM component has been discussed to reflect the chloroplast movement in the light (Cazzaniga et al., 2013).

Grana are thylakoid structures that develop primarily in land plants. It is thought that LHCIIs play a role in grana biogenesis because mutants or transgenic plants in which the accumulation or organization of LHCIIs is altered show disturbances of grana structure (Labate et al., 2004; Kim et al., 2009; Cui et al., 2011; Pietrzykowska et al., 2014). The charged stroma-facing surface of LHCIIs interacts via the same surface on other molecules present in a different membrane, likely resulting in cohesion of the two membranes (Standfuss et al., 2005). Kinase mutants defective in phosphorylation of LHCIIs and PSII subunits exhibit reduced stacking of grana (Fristedt et al., 2009), demonstrating that LHCIIs phosphorylation is also critical for the stacking of grana. CURVATURE THYLAKOID1 (CURT1) has recently been identified as another protein required for grana stacking and acts independently of the mechanism mediated by LHCIIs. CURT1 proteins are localized to the grana margin and probably determine the diameter of the grana disc by causing membrane curvature. The *Arabidopsis thaliana curt1* mutants have pseudograna, which consist of reduced numbers of thylakoid discs having enlarged diameters and greatly reduced marginal regions, but the accumulation of PSII subunits or LHCIIs is unaltered in these mutants (Armbruster et al., 2013; Pribil et al., 2014). Details of the molecular mechanism of grana formation, the thylakoid architecture, and their functional link with photosynthesis and its regulatory processes are not yet fully understood.

Here, we identified two Arabidopsis mutants exhibiting low levels of NPQ induction and thus called them *reduced induction of non-photochemical quenching1* (*riq1*) and *riq2*. We initially focused on these genes in a proteomics approach to clarify the components of PSI cyclic electron transport that depend on PROTON GRADIENT REGULATION5 (PGR5), but we later recognized that they were not related to PGR5. Actually, in *riq* mutants, the grana were stacked more highly than those in the wild type. Our analyses revealed that RIQ proteins contribute to NPQ and grana stacking in ways different from those of CURT1 functions. This study provides genetic evidence for the functional link between grana structure and organization of LHCIIs, which are shown to be related to qE induction and state transitions.

RESULTS

Arabidopsis *riq* Mutants Cannot Sustain NPQ under Moderate Light

Arabidopsis RIQ1 and RIQ2 contain 158 and 198 amino acid residues, respectively, and share a conserved domain of unknown function (DUF) 1118, which includes two putative transmembrane domains. Their N-terminal regions were predicted to be transit peptides targeted toward chloroplasts (Figure 1A). No other genes in the Arabidopsis genome encode proteins similar to RIQ. *RIQ* genes are conserved in land plants and some green eukaryotic algae, including *Chlorella variabilis*. However, only the *RIQ1* ortholog was identified in *Micromonas pusilla RCC299*, one of the dominant photosynthetic eukaryotes in marine ecosystems (Figure 1B), and *Chlamydomonas reinhardtii* and *Volvox carteri* do not contain *RIQ*-related genes, implying that some green algal lineages have lost them.

We investigated the phenotypes of the Arabidopsis T-DNA insertional mutants of *riq1* and *riq2*. In *riq1*, T-DNA was inserted into the first exon of *RIQ1*, whereas in *riq2*, it was inserted into the 5′ untranslated region of *RIQ2* (Figure 1C). RT-PCR analyses did not detect *riq* transcripts in either mutant, suggesting that both alleles were null (Figure 1D). In *riq* mutants, including the double mutant *riq1 riq2*, there was no mutant phenotype for growth (Figure 1E), chlorophyll content, or chlorophyll *a*/*b* ratio (Supplemental Table 1) under the growth conditions used in this study. The maximum photochemical efficiency of PSII (Fv/Fm), which is often used to estimate the PSII photoinhibition, was the same (0.77) among the genotypes ($n = 3$).

However, a mutant phenotype was detected in both *riq1* and *riq2* in an analysis of chlorophyll fluorescence. Steady state NPQ levels were mildly but significantly lower in *riq1* and *riq2* than in the wild type, although they were higher than those in *npq4*, which is defective in PsbS (Li et al., 2000) (Figure 2A). To characterize this phenotype in more detail, induction of NPQ was measured at various white actinic light (AL) intensities, where photosynthesis was activated. At 1900 μmol photons m^{-2} s^{-1}, NPQ induction was nearly unaffected in *riq1* and *riq2*, reaching 2.0 by 5 min in the light (Figure 2B). In wild-type plants exposed to AL at 250 μmol photons m^{-2} s^{-1}, NPQ peaked at 1.4 within 5 min. By contrast, in *riq1* and *riq2*, the maximum level (1.1) of NPQ was induced after a 2-min exposure to AL and was followed by a gradual reduction in the light to 1.0 after 5 min (Figure 2C). Under a lower AL intensity of 100 μmol photons m^{-2} s^{-1}, NPQ induction was also transient in the wild type, perhaps because of the relaxation of ΔpH by ATP synthase. However, the relaxation of NPQ in the light was faster in *riq1* and *riq2* than in the wild type (Figure 2D). To confirm that the NPQ phenotypes were due to the *riq* defects, *RIQ* genes were introduced into the mutants under the control of their own promoters. This transformation induced the recovery of NPQ levels at 250 μmol photons m^{-2} s^{-1} (Supplemental Figure 1). A similar NPQ phenotype was observed under red AL (Supplemental Figure 2), suggesting that the blue-light-dependent chloroplast movement monitored as qM (Cazzaniga et al., 2013) was not affected.

Despite the high level of sequence identity, both *riq1* and *riq2* exhibited a similar NPQ reduction (Figure 2), suggesting that the RIQ1 and RIQ2 functions were not redundant. However, it is still possible that their functions partly overlap. To test this possibility, NPQ induction was analyzed in *riq1 riq2*. The phenotypes of *riq1 riq2* were identical to those of the single mutants in terms of both light intensity dependence (Figure 2A) and the time courses of induction and relaxation (Figures 2C and 2D), suggesting that RIQ1 and RIQ2 played nonredundant roles in contributing to NPQ.

RIQ1 and RIQ2 Are Localized in the Grana Core

To localize RIQ proteins, the specific antibodies recognizing the predicted mature forms of each protein were prepared. Both RIQ1 and RIQ2 were found in the membrane fraction isolated from the wild type but were absent in the corresponding single mutant

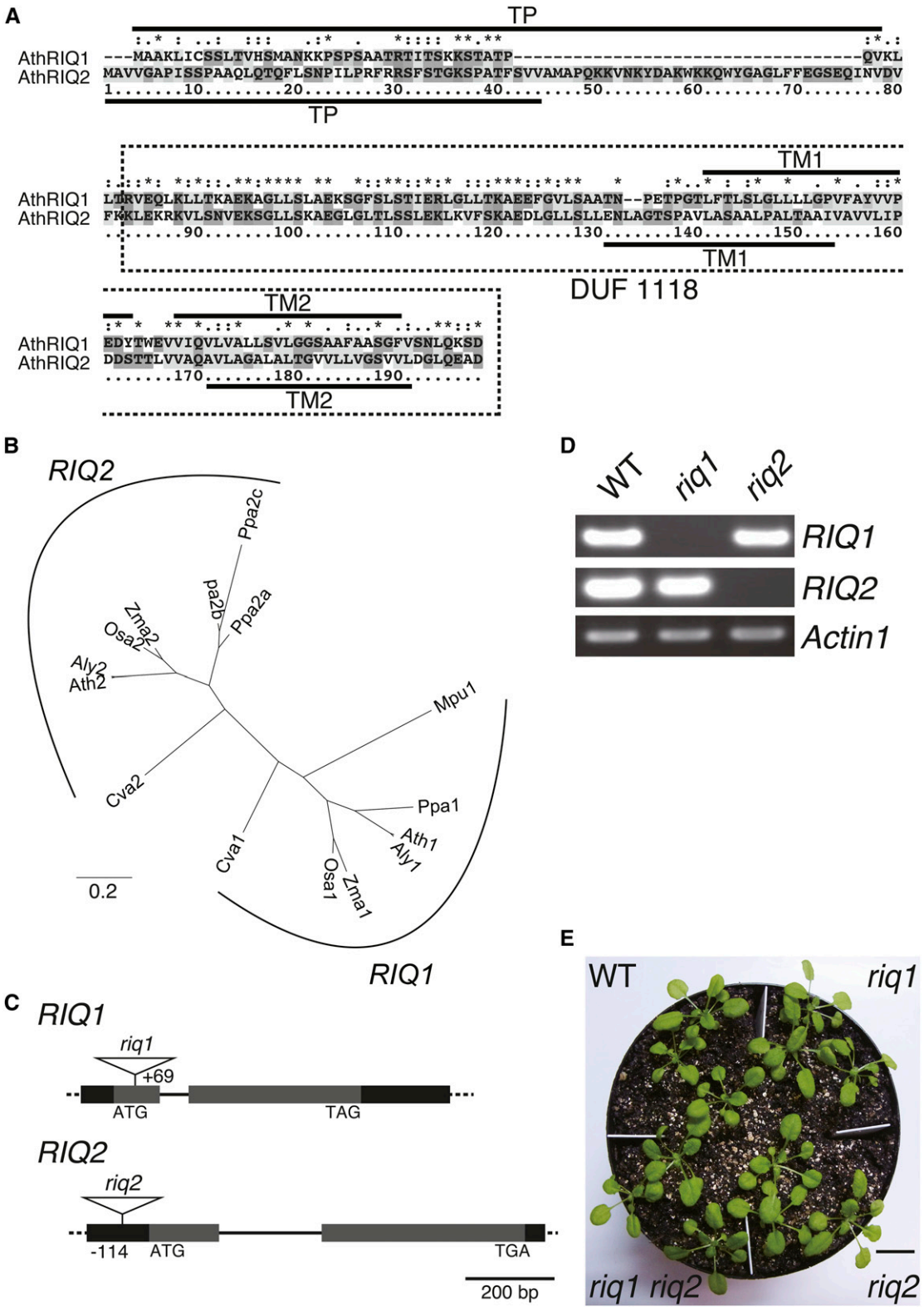

Figure 1. Characteristics of *RIQ1* and *RIQ2* and Their Arabidopsis T-DNA Knockout Mutants.

(A) Alignment of proteins encoded by Arabidopsis (Ath) *RIQ1* and *RIQ2*. Transit peptides targeted toward plastids (TP) and transmembrane domains (TM1 and TM2) are indicated by bold horizontal lines. The dotted box represents DUF1118. Asterisks, colons, and periods above the alignment indicate identical residues, and strongly and weakly conservative replacements.

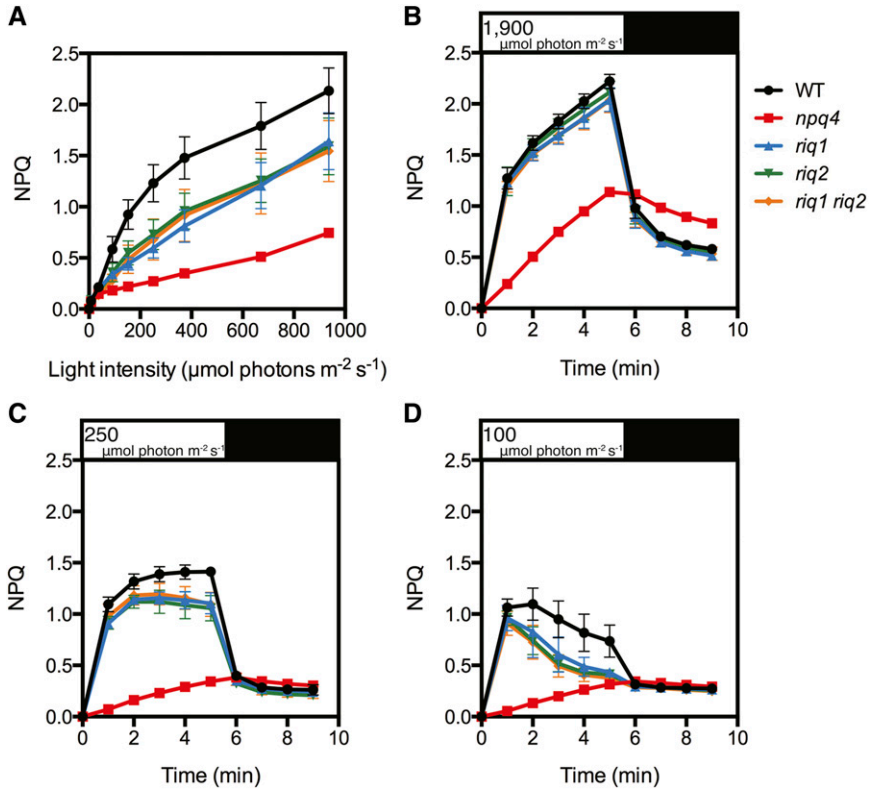

Figure 2. Decrease of NPQ Induction Measured in *riq* Mutants.

(A) Dependence of NPQ on light intensity. Data are means ± SD (n = 5).
(B) to **(D)** Time course of NPQ induction in plants irradiated with 1900 μmol photons m^{-2} s^{-1} **(B)**, 250 μmol photons m^{-2} s^{-1} **(C)**, or 100 μmol photons m^{-2} s^{-1} **(D)**. After a 30-min dark adaptation, actinic light was applied for 5 min (white boxes) and was then followed by 4 min in the dark for relaxation of qE (black boxes). Data are means ± SD (n = 3).

(Figure 3A). Subfractionation of chloroplasts into the chloroplast envelope, thylakoid, and stromal fractions revealed the specific localization of the RIQ proteins to the thylakoid membrane (Figure 3B), consistent with information in the Plant Proteome Database (Sun et al., 2009). The anti-RIQ1 antibody detected two signals that were absent in *riq1* and *riq1 riq2* (Figure 3A). The upper, faint signal was unlikely to be due to nonspecific reaction of the antibody because the same signal was detected using independently prepared antibody raised against a RIQ1 oligopeptide (EEFGVLSAATNPET) (Supplemental Figure 3). Although the RIQ1 level was unaffected in *riq2*, in *riq1* the RIQ2 level was reduced to ~25% of that in the wild type (Figure 3A), suggesting that RIQ1 is required for RIQ2 accumulation. Protein accumulation was restored to nearly the wild-type level by introduction of *RIQ1* or *RIQ2* into the corresponding mutant (Figure 3A).

The protein compositions of the grana and the stromal lamella differ strikingly in chloroplasts of land plants (Dekker and Boekema, 2005). The grana margin is the edge region of the grana thylakoid and is rich in CURT1 family proteins (Armbruster et al., 2013; Puthiyaveetil et al., 2014). To clarify the localization of RIQ proteins in the thylakoid membrane, these membranes were subfractionated into the grana core, grana margin, and stromal lamella. Both RIQ1 and RIQ2 were detected mainly in the grana core, as was PsbO (a PSII subunit). A trace amount of RIQ2 was

Figure 1. (continued).

(B) An unrooted phylogenetic tree of RIQ orthologs from Arabidopsis (Ath), *Arabidopsis lyrata* (Aly), *Oryza sativa* (Osa), *Zea mays* (Zma), *Physcomitrella patens* (Ppa), *Chlorella variabilis* (Cva), and *Micromonas pusilla* RCC299 (Mpu). The tree was constructed by MrBayes 3.2 (Ronquist and Huelsenbeck, 2003) with the 1000 bootstrap trials.
(C) Schematic structural models of *RIQ1* and *RIQ2*. Black boxes, untranslated region; gray boxes, coding regions of exons; solid lines, introns; dotted lines, noncoding regions out of the UTRs. Positions of the T-DNA insertion are indicated for *riq1* and *riq2*.
(D) RT-PCR analysis of *RIQ1* and *RIQ2* transcripts in wild-type, *riq1*, and *riq2* plants. *Actin1* (*AT2G37620*) mRNA was used as a loading control.
(E) Growth phenotype of the wild type, *riq1*, *riq2*, and *riq1 riq2*. Plants were cultured at 50 μmol photons m^{-2} s^{-1} in growth chamber conditions for 3 weeks. Bar = 1 cm.

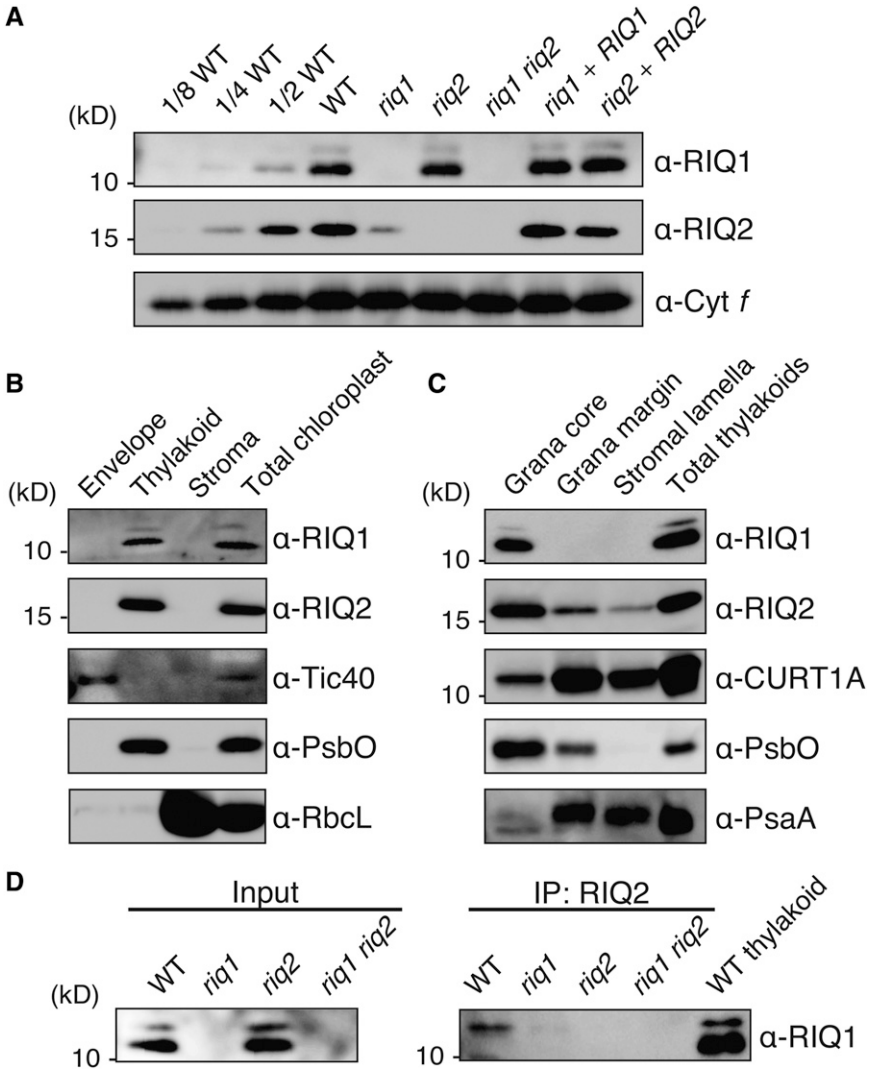

Figure 3. RIQ1 and RIQ2 Are Grana-Localized Proteins.

(A) Immunodetection of RIQ proteins in the wild type, *riq* mutants, and their complemented lines. Fractions indicate 2-fold dilution of the wild type. A chloroplast membrane protein extract corresponding to 2 μg chlorophyll was loaded onto each lane, as were a series of dilutions of wild-type thylakoids. Cyt *f* was detected as a loading control. In all figure parts, antibodies used are shown to the right of the immunoblots, and molecular mass markers in kilodaltons are shown to the left.

(B) Separation of wild-type chloroplasts into fractions of envelope, thylakoid, and stroma followed by immunodetection of RIQ proteins. Tic40 (envelope), PsbO (thylakoid), and RbcL (stroma) were detected as markers of chloroplast fractionation. Molecular mass markers in kilodaltons are shown to the left.

(C) Separation of wild-type thylakoids into fractions of grana core, grana margin, and stromal lamella, followed by immunodetection of RIQ proteins. PsbO (grana core), CURT1A (grana margin), and PsaA (stromal lamella) were detected as markers for membrane fractionation. Molecular mass markers in kilodaltons are shown to the left.

(D) Coimmunoprecipitation analysis. Chloroplast membranes isolated from wild-type, *riq1*, *riq2*, and *riq1 riq2* leaves were solubilized for application to beads to which polyclonal RIQ2 antibody was attached (Input). After washing of the beads, coimmunoprecipitated proteins (IP) were eluted and analyzed by immunodetection with antibody raised against the recombinant RIQ1. Molecular mass markers in kilodaltons are shown to the left.

also detected in the grana margin and stromal lamella fractions (Figure 3C).

Both RIQ1 and RIQ2 Are Required for Full Induction of NPQ

It is possible that RIQ1 is required just to stabilize RIQ2 (Figure 3A) and that the reduction of NPQ observed in *riq1* (Figure 2) occurs via the reduced level of RIQ2. To test this possibility, we expressed *RIQ2* under the control of the CaMV 35S promoter in *riq1*. If this possibility were true, then the *riq1* NPQ phenotype would be complemented by the accumulation of RIQ2 to wild-type level even in the absence of RIQ1. We obtained four transgenic lines, two of which accumulated wild-type level of RIQ2 (Figure 4A). All the lines exhibited NPQ levels similar to those of *riq1* (Figure 4B).

This result suggests that both RIQ1 and RIQ2 are required for full induction of NPQ.

RIQ1 is required for RIQ2 accumulation, and both proteins are required for the normal NPQ induction (Figures 3A and 4). To test the possibility that RIQ1 and RIQ2 interact in vivo, coimmunoprecipitation was performed using a polyclonal antibody against RIQ2. As a negative control, *riq2*, which accumulated the wild-type level of RIQ1, was used. In the wild type, only the RIQ1 signal with slower mobility was detected in the immunoprecipitate (Figure 3D), suggesting that at least the major form of RIQ1 did not interact with RIQ2.

riq Mutants Are Not Defective in the Known qE Machinery

Production of qE is induced by lumenal acidification and is dependent on the trans-thylakoid proton gradient (ΔpH) (Horton et al., 1996; Li et al., 2009). The *riq* NPQ phenotype (Figure 2) may be due to a defect in the qE machinery that senses lumenal acidification and induces NPQ. Alternatively, the defect may affect the mechanism of ΔpH formation or maintenance. The electron transport rate reflects the relative rate of electron transport through PSII and was not significantly affected in any genotypes (Supplemental Figure 4A). Another parameter, 1-qL, which represents the state of reduction of the plastoquinone pool, was slightly but not significantly higher in *riq* mutants than in the wild-type (Supplemental Figure 4B).

Chlorophyll fluorescence analysis implied that *riq* mutants were defective in the qE machinery rather than in the formation or maintenance of ΔpH. To test this more directly, we measured the amplitude of the total light-dark difference in the electrochromic shift signal (ECS_t), which reflects the total size of the proton motive force (*pmf*) formed in the light. The *pmf* was saturated at 249 μmol photons m^{-2} s^{-1} in the wild type. As reported previously (Wang et al., 2015), the *pmf* was significantly lower in *pgr5* than in the wild type under AL of 249 and 1707 μmol photons m^{-2} s^{-1}. However, the size of the *pmf* was not affected in *riq* mutants (Supplemental Figure 5), suggesting that the NPQ phenotype is not due to a reduced ΔpH.

Even with sufficient ΔpH, a defect in proteins associated with the qE machinery, such as PsbS, CP26, and CP29, impairs qE induction (Li et al., 2000; de Bianchi et al., 2008, 2011). Accumulation of these proteins was not reduced in *riq* mutants, and subunit levels of the other thylakoid protein complexes were also unaffected (Supplemental Figure 6). To assess the possibility that the xanthophyll cycle involved in qE (Niyogi et al., 1998) is affected in *riq* mutants, we analyzed the carotenoid conversion induced by high light using HPLC. In the wild type, the deepoxidation state of xanthophyll carotenoids was low in the dark but was elevated to ~30 in the light (Supplemental Figure 7). Under high light, deepoxidation state of xanthophyll carotenoids was not affected in *riq1* or *riq2*, indicating that the NPQ phenotype in *riq* mutants cannot be explained by reduced activity of the xanthophyll cycle (Supplemental Figure 7). Taken together, these findings show that the NPQ phenotype in *riq* mutants is not caused by defects in *pmf* regulation, accumulation of NPQ-related proteins, or xanthophyll cycle activity.

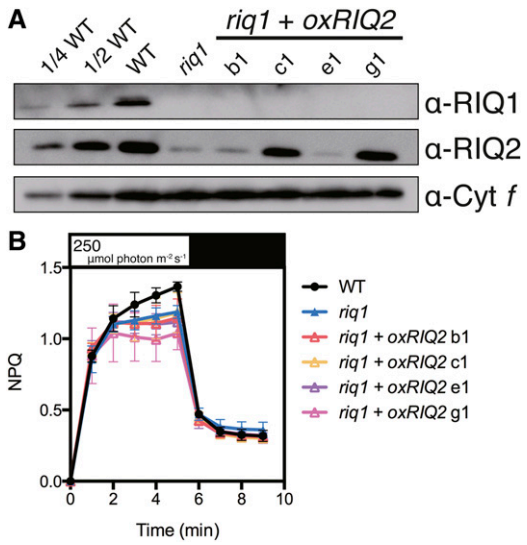

Figure 4. Wild-Type Level of RIQ2 Did Not Complement the NPQ Phenotype of *riq1*.

(A) Immunodetection of RIQ1 and RIQ2 in the wild type, *riq1*, and four independent *RIQ2* complementation lines in the *riq1* background. A chloroplast membrane protein extract corresponding to 2 μg chlorophyll was loaded onto each lane, as were a series of 2-fold dilutions of wild-type thylakoids. Antibodies used are shown to the right of the immunoblots. Cyt *f* was detected as a loading control.

(B) Time course of NPQ induction measured at 250 μmol photons m^{-2} s^{-1}. After a 30-min dark adaptation, actinic light was applied for 5 min (white box) and was then followed by 4 min in the dark for relaxation of qE (black box). This experiment used other leaves of the same plants used in part **(A)**. Data are means ± SD (n = 3).

LHCIIs Are Required for RIQ-Related NPQ

In Arabidopsis, the main component of NPQ is qE, reflecting the size of thermal dissipation from LHCIIs (Johnson et al., 2011). In *riq* mutants, accumulation of LHCIIs (Lhcb1 to 6) was not affected (Supplemental Figure 6), consistent with them having a normal chlorophyll *a*/*b* ratio (Supplemental Table 1). To determine whether LHCIIs were involved in RIQ-related NPQ in vivo, we crossed *riq* mutants with *chlorina1-1* (*ch1-1*), which was defective in chlorophyll *b* synthesis (Murray and Kohorn, 1991; Espineda et al., 1999). Because of the absence of chlorophyll *b*, *ch1-1* does not accumulate any functional LHCIIs except for Lhcb5, resulting in a drastic reduction in qE (Havaux et al., 2007; Takabayashi et al., 2011). The small amount of NPQ remaining in *ch1-1* is considered to be related to Lhcb5 and the PSII core (Havaux et al., 2007). Accumulation of RIQ proteins was not affected in *ch1-1* (Figure 5A), suggesting that RIQ proteins accumulate independently of LHCIIs. At 250 μmol photons m^{-2} s^{-1}, in which the reduced size of NPQ was evident in *riq* mutants, a similar level of NPQ was induced among *ch1-1*, *riq1 ch1-1*, and *riq2 ch1-1* (two independent lines) (Figures 5B and 5C). The *riq* defects did not affect the NPQ induction remaining in *ch1-1*. This indicates that RIQ proteins are required for efficient thermal dissipation from LHCIIs, although the stability of RIQ proteins is independent from LHCII accumulation.

Organization of LHCIIs Is Affected in *riq* Mutants

Induction of qE is related to partial disassociation of LHCIIs, which forms two quenching sites (Holzwarth et al., 2009; Johnson et al., 2011). To analyze the impact of the *riq* defects on the PSII-LHCIIs structure in vivo, the antenna size per PSII reaction center was measured using a flash fluorescence induction method. In this assay, a saturating flash was applied to a solution containing isolated thylakoids treated with DCMU, an inhibitor to block electron transfer from PSII to the plastoquinone pool, to monitor an increase in chlorophyll fluorescence from LHCIIs at high time resolution. The time required to reach the maximum level is proportional to the size of the antennae connected to the PSII reaction center (Nedbal et al., 1999). *riq* mutants had slower fluorescence induction kinetics than the wild type (Figure 6A), suggesting that they had smaller PSII antennae per reaction center. Consistent with the NPQ phenotype, *riq1 riq2* had a phenotype similar to that of the single mutants (Figure 6A).

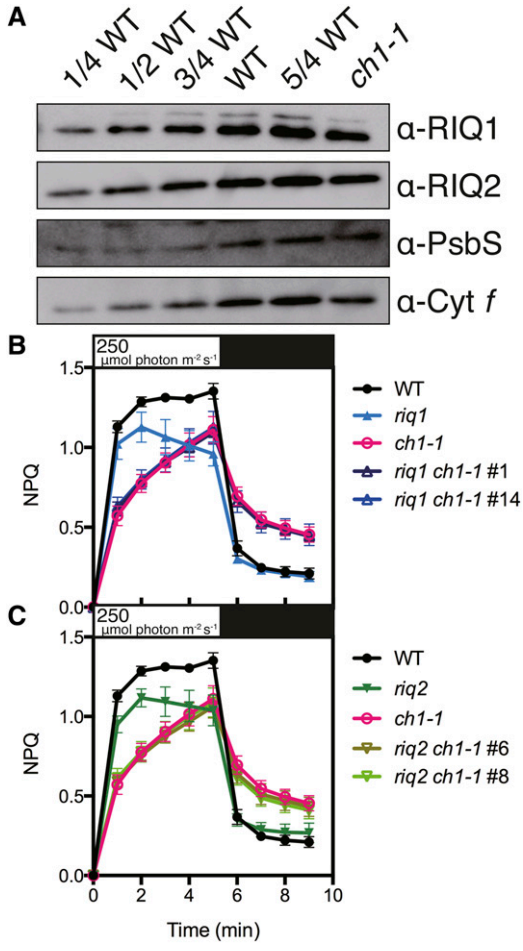

Figure 5. LHCIIs Are Required for RIQ-Related NPQ.

(A) Immunodetection of RIQ1, RIQ2, and PsbS proteins in the wild type and *ch1-1*. A chloroplast membrane protein extract was loaded onto the wild-type and *ch1-1* lanes on the basis of equal total protein amounts, as were several dilutions of wild-type thylakoids. Antibodies used are shown to the right of the immunoblots. Cyt *f* was used as a loading control.
(B) and **(C)** Time course of NPQ induction in the wild type, *riq1*, *ch1-1*, and *riq1 ch1-1* #1 and #14 **(B)** and the wild type, *riq2*, *ch1-1*, and *riq2 ch1-1* #6 and #8 **(C)** was measured at 250 µmol photons m^{-2} s^{-1}. After 30 min of dark adaptation, actinic light was applied for 5 min (white boxes) and then was followed by a 4-min dark period for the relaxation of qE (black boxes). Data are means ± SD (n = 4).

To test the possibility that *riq* mutants were defective in the reorganization process of LHCIIs, we analyzed chlorophyll fluorescence at 77K to test their capacity for state transitions. At the temperature, chlorophyll fluorescence is emitted from both photosystems, and its level represents the size of antennae attached to each photosystem. After dark adaptation, leaves were exposed to weak red light to induce state 2, where phosphorylated LHCIIs dissociated from PSII and associated to PSI, and far-red light to induce state 1, where dephosphorylated LHCIIs reassociated to PSII (Minagawa, 2013). This artificial induction of state 1 or state 2 was followed by being immediately soaked in liquid nitrogen for fluorescence measurement. In the spectra normalized at the emission peak from PSI (736 nm), wild-type leaves showed a clear difference in fluorescence between state 1 and state 2 at around 685 to 695 nm, corresponding to the fluorescence emitted from the PSII antennae (Figure 6B). This difference reflects the change in antenna size based on state transitions (Fleischmann et al., 1999). Arabidopsis *stn7* was fixed in state 1 (Bellafiore et al., 2005) and showed no fluorescence change between the two light conditions (Figure 6C). Although *riq* mutants maintained their state transition activity, the amplitudes of the fluorescence changes were smaller than those in the wild type (Figures 6E to 6G), indicating that state transitions were greatly impaired in *riq* mutants. Immunodetection using a specific antibody against phosphorylated proteins revealed that the phosphorylation levels of LHCIIs isolated from leaves in which state 2 was induced did not differ among the wild type and *riq* mutants, but it did differ in *stn7* (Supplemental Figure 8). In state 1, LHCIIs were dephosphorylated in *riq* mutants, as in the wild type. This result suggests that the inhibition of state transitions observed in *riq* mutants was not induced via alteration of phosphorylation or dephosphorylation of PSII subunits or LHCIIs.

Grana Stacking Is Enhanced in *riq* Mutants

The stacking level of the grana thylakoid is closely related to the mobility of proteins localized to the region (Dekker and Boekema, 2005; Pribil et al., 2014). We used transmission electron microscopy to compare thylakoid architecture among the wild type and *riq* mutants. Consistent with the observed normal plant growth (Figure 1E), the thylakoid structure was not seriously disturbed in *riq* mutants (Figures 7A to 7D; Supplemental Figure 9). However, the grana were more stacked than those in the wild type; this observation was supported statistically by an analysis of the number of thylakoid stacks in the grana region (Figure 7E). Consistent with the NPQ phenotype (Figure 2) and the reduction in antenna size (Figure 6A), *riq1 riq2* had a phenotype similar to that of the single mutants (Figure 7D; Supplemental Figure 9), suggesting that function of RIQ1 and RIQ2 was also not redundant in thylakoid stacking.

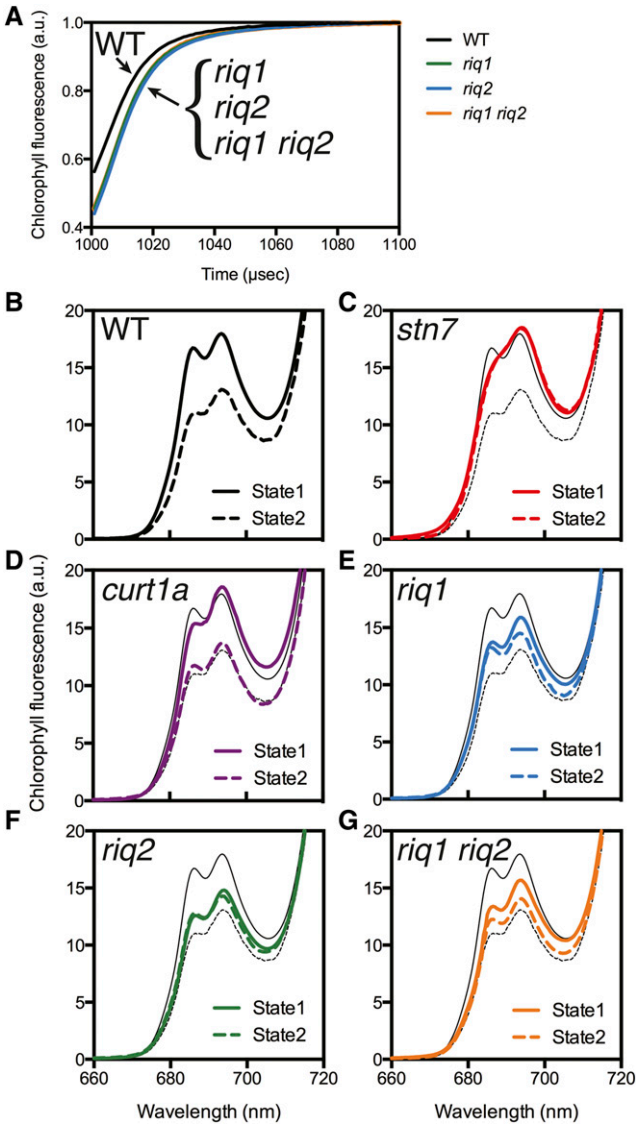

Figure 6. Smaller Antenna Size of PSII and Impaired State Transition Activity in *riq* mutants.

(A) Flash fluorescence induction analysis of the wild type and *riq* mutants. The time course of fluorescence increase during a saturating flash was monitored. Slower induction of fluorescence indicates that smaller light-harvesting antennae are connected to the PSII core. The *x* axis shows the time after application of a saturating flash. Transient amplitudes of fluorescence were normalized against maximum levels of fluorescence. Lines represent the averages of four biological replicates.

(B) to **(G)** Chlorophyll fluorescence analysis. Intensities of chlorophyll fluorescence (660 to 720 nm) at 77K in state 1 (solid lines) and state 2 (dotted lines) in the wild type **(B)**, *stn7* **(C)**, *curt1a* **(D)**, *riq1* **(E)**, *riq2* **(F)**, and *riq1 riq2* **(G)**. Fluorescence levels were normalized against the maximum intensity of the fluorescence at 736 nm that was emitted from PSI. In the graphs **(C)** to **(G)**, wild-type fluorescence levels in state 1 and state 2 were shown as black thin solid and dotted lines, respectively.

RIQ and CURT1 Proteins Are Independently Required to Sustain NPQ Levels

RIQ proteins may be associated with the organization of LHCIIs via optimization of the level of grana stacking. A similar link between grana structure and NPQ has been reported in *curt1a*. Because CURT1 proteins contribute to grana formation by inducing membrane curvature (Armbruster et al., 2013), defects in them result in a thylakoid phenotype (a lack of normal grana stacking) that contrasts with that in *riq* mutants. Armbruster et al. (2013) also reported a reduction in NPQ in *curt1a*, but the reason for this phenotype remains unclear. To study the possible link between thylakoid structure and the function of LHCIIs, we included *curt1a* in our analyses. In this study, we used a new *curt1a* allele obtained from the Arabidopsis Biological Resource Center (Supplemental Figure 10A). *CURT1A* transcripts were not detected in the mutant (Supplemental Figure 10B), indicating that *curt1a* is a knockout allele. Introduction of the *CURT1A-HA* gene complemented the *curt1a* mutant phenotypes regarding the protein level and NPQ induction (Supplemental Figures 10C and 10D). Figure 8A shows the time course of NPQ induction at 250 μmol photons m^{-2} s^{-1}. As in *riq* mutants, NPQ was transiently induced in *curt1a* to the wild-type level (1.2) within 2 min of exposure to light. However, no further increase in NPQ was induced, resulting in a slight decline in NPQ levels during an additional 3 min in the light. This *curt1a* phenotype in NPQ was similar to that observed in *riq* mutants (Figure 8A). To analyze the genetic interaction between *riq* and *curt1a* mutants, we created double mutants. In *riq1 curt1a* and *riq2 curt1a*, the NPQ level was further decreased compared with that in the single mutants (Figure 8A), suggesting that RIQ and CURT1 affect NPQ in different pathways. Consistently, the *curt1a* defect did not affect the RIQ levels and the *riq* defects did not affect the CURT1A level (Supplemental Figure 6).

To investigate the phenotype of NPQ induction in *riq* and *curt1a* mutants in more detail, NPQ induction and relaxation were monitored during 5 min of light (250 μmol photons m^{-2} s^{-1}) and 1-min dark cycles. In the wild type, a high level of NPQ was induced during the first min in the second light period (Figure 8B), whereas *riq* or *curt1a* mutants showed a much lower level of NPQ. The same trend was observed in the third light period. This phenotype was more evident in *riq1 curt1a* and *riq2 curt1a* than in the single mutants (Figure 8B) but was different using a longer dark interruption (10 min). As was the case with the initial light period (0 to 5 min), a high level of NPQ was transiently induced in all genotypes, including the double mutants, during the first 1 min in the second light period (15 to 20 min) after the long dark period (Figure 8C). In both *riq* and *curt1a* mutants, the ability to induce high levels of NPQ (more than 1.5) transiently was recovered during the 10-min dark adaptation.

Synergistic Effects of the *riq* and *curt1a* Mutations on Thylakoid Structure

The *riq* and *curt1a* mutants exhibited opposite mutant thylakoid structure phenotypes (Figure 7; Armbruster et al., 2013), although the NPQ induction phenotypes were similar (Figure 8A). To study the link between thylakoid structure and the organization of LHCIIs, we used electron microscopy to observe chloroplasts of

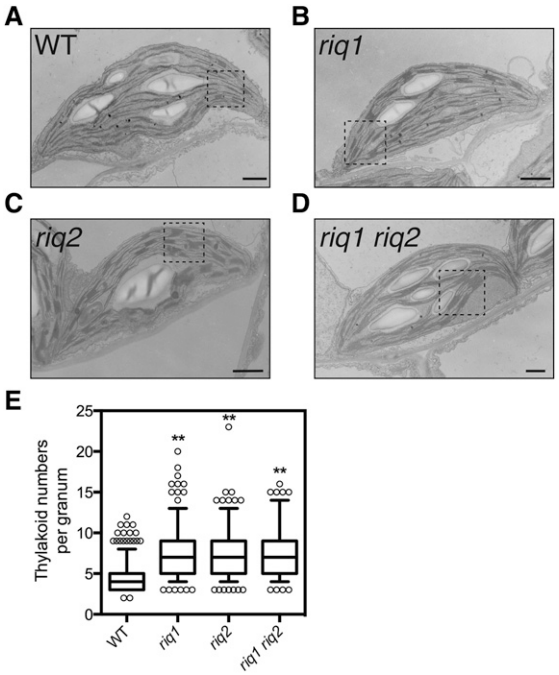

Figure 7. Increased Stacking of Grana Thylakoids of *riq* Mutants.

(A) to **(D)** Chloroplast ultrastructures of the wild type **(A)**, *riq1* **(B)**, *riq2* **(C)**, and *riq1 riq2* **(D)**. Dotted squares represent the regions of the magnified images shown in Supplemental Figures 9E to 9H. Bars = 1 μm.

(E) Quantitative comparison of the number of thylakoid membranes per granum. Grana stacks were randomly chosen from different chloroplasts to count the thylakoid number per granum. For plotting the numbers, boxes extend from the 25th to 75th percentiles. Lines in the middle of the box are plotted at the median. Whiskers are drawn down to the 5th percentile and up to the 95th. Points below and above the whiskers are drawn as individual dots. **P < 0.01, significant by one-way ANOVA (Dunnett's post hoc test versus the wild type). *n* (the number of grana stacks measured) = 192 to 394.

riq curt1a double mutants. Consistent with previous reports (Armbruster et al., 2013; Pribil et al., 2014), fewer stacked grana structures, with significantly increased diameters, were formed in *curt1a* (Figures 9A to 9D; Supplemental Figures 11A to 11D). In *riq1 curt1a*, the grana were similarly elongated but their stacking was enhanced, as in *riq* single mutants (Figures 9E and 9F; Supplemental Figure 11E). This finding was supported by a quantitative analysis of grana stacking (Figure 9I). Notably, the mutant phenotype for thylakoid structure in *riq2 curt1a* was synergistic rather than additive. At the distal parts of the lens-shaped structure in *riq2 curt1a*, the thylakoids were abnormally stacked and aggregated (black arrowheads in Figures 9G and 9H; Supplemental Figure 11F). Probably because of the disturbance of the thylakoid structure, the chloroplast envelope was unusually wavy (white arrowheads in Figures 9G and 9H; Supplemental Figure 11F). Holes were detected in the stroma, reflecting dents in the envelope (asterisks in Figure 9G; Supplemental Figure 11F).

Consistent with the phenotype observed in NPQ induction (Figure 2) and stacking of the grana in the *riq* single mutant (Figure 7), the analysis of the double mutants with *curt1a* suggested that RIQ1 and RIQ2 had nonoverlapping functions. The function of RIQ1 was not only required to accumulate RIQ2 but also essential to fully induce NPQ (Figures 3A and 4). However, it is still possible that the phenotype observed in the thylakoid structure was caused solely by the reduced RIQ2 level. If this were the case, the

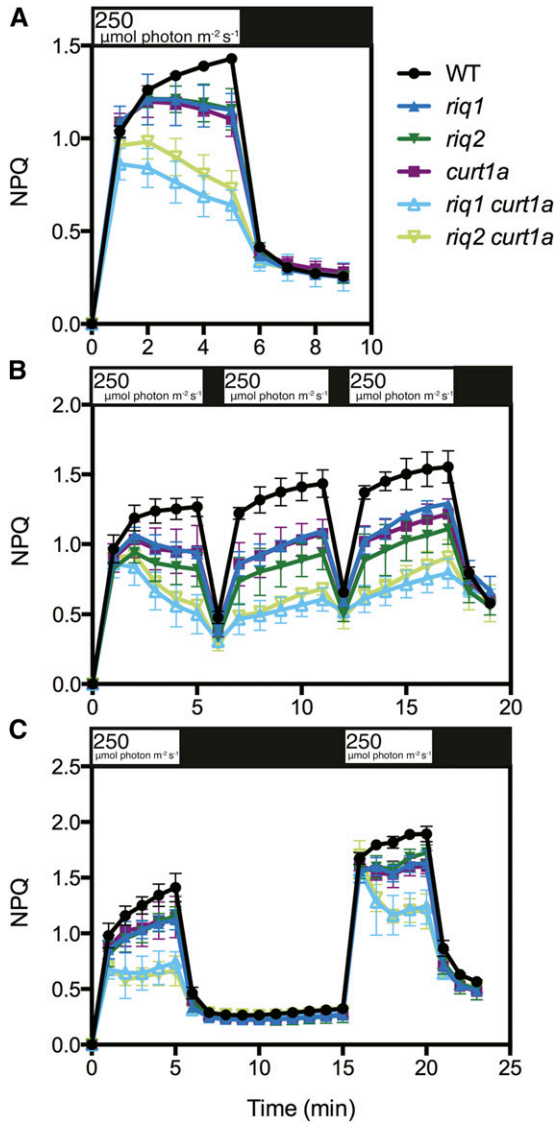

Figure 8. Enhanced NPQ Phenotype of *riq curt1a* Double Mutants.

(A) Time course of NPQ induction in the wild type, *riq1*, *riq2*, *curt1a*, *riq1 curt1a*, and *riq2 curt1a*, as measured at 250 μmol photons m^{-2} s^{-1}. After 30 min of dark adaptation, AL was applied for 5 min (white box); this was followed by a 4-min dark period for relaxation of qE (black box). Data are means ± SD (*n* = 3).

(B) and **(C)** Time course of NPQ induction and relaxation in *riq* and *curt1a* single mutants and their double mutants.

(B) A combination of 5 min of AL treatment (white boxes; 250 μmol photons m^{-2} s^{-1}) plus 1 min of dark interruption (black boxes) was applied three times.

(C) Two 5-min AL exposures (white boxes; 250 μmol photons m^{-2} s^{-1}) were interrupted by a 10-min dark period (black box). Data are means ± SD (*n* = 3).

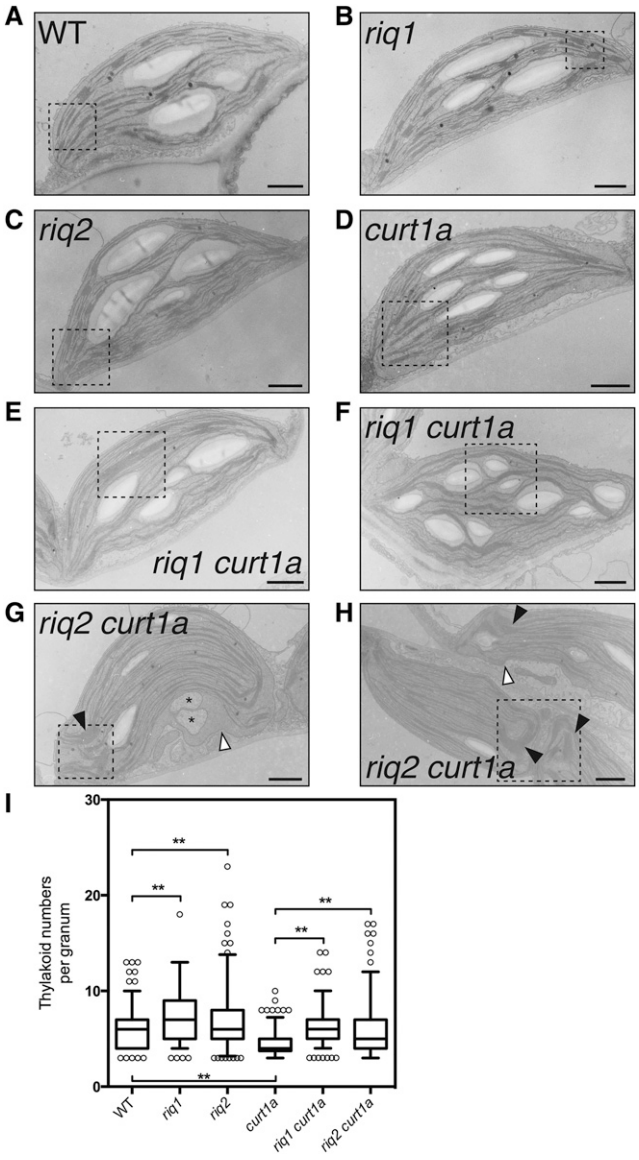

Figure 9. Thylakoid Structures Were Additively and Synergistically Disturbed in *riq1 curt1a* and *riq2 curt1a*, Respectively.

(A) to **(H)** Chloroplast ultrastructures of the wild type **(A)**, *riq1* **(B)**, *riq2* **(C)**, *curt1a* **(D)**, *riq1 curt1a* (**[E]** and **[F]**), and *riq2 curt1a* (**[G]** and **[H]**). In **(G)** and **(H)**, abnormally aggregated thylakoids and wavy envelopes are indicated by black and white arrowheads, respectively. Unusual holes in the stroma (reflecting dents in the envelopes) are indicated by asterisks. Dotted squares represent the regions of the magnified images shown in Supplemental Figures 11G to 11N. Bars = 1 μm.

(I) Quantitative comparison of the number of thylakoid membranes per granum. Grana stacks were randomly chosen from different chloroplasts to count the thylakoid number per granum. For plotting the numbers, boxes extend from the 25th to 75th percentiles. Lines in the middle of the box are plotted at the median. Whiskers are drawn down to the 5th percentile and up to the 95th. Points below and above the whiskers are drawn as individual dots. **$P < 0.01$, significant by one-way ANOVA (Dunnett's post hoc test versus the wild type or *curt1a*). *n* (the number of grana stacks measured) = 152 to 186.

different phenotypes observed in *riq1 curt1a* and the *riq2 curt1a* would be explained by the different levels of RIQ2 independently of RIQ1. To test this possibility, the thylakoid architecture of the RIQ2-complemented *riq1* plants, which accumulated wild-type level of RIQ2 in the absence of RIQ1, was analyzed (Figure 4A). Two transgenic lines exhibited the same level of grana stacking as did the nontransgenic *riq1* mutant (Figure 10). Therefore, RIQ1 is also required for the optimization of grana stacking, independently of its requirement for the accumulation of RIQ2, as was observed in NPQ induction (Figure 4B).

DISCUSSION

Although the exact molecular mechanism is unclear, *riq* mutants may not be able to stably sustain the quenching mode of LHCIIs. This idea is supported by the following observations: (1) antenna size per PSII reaction center was smaller in *riq* mutants than in the wild type (Figure 6A); and (2) state transitions were greatly restricted in *riq* mutants (Figures 6B to 6G). The *riq* mutants were locked in an intermediate state and could not respond to light conditions inducing state transitions. Some of LHCIIs may not be associated with PSII in state 1; this is consistent with the smaller antenna size of PSII (Figure 6A). A critical event during qE induction is the dynamic reorganization of LHCIIs, resulting in their partial dissociation from PSII and aggregation in the grana to form quenching sites (Holzwarth et al., 2009; Johnson et al., 2011). This organization process was affected in *riq* mutants, likely because some LHCIIs were not functionally associated with PSII to stabilize the quenching mode of LHCIIs in the light. This was supported by the fact that NPQ reduction measured in *riq* mutants was not detected in the double mutants with *ch1-1* (Figure 5).

What is the link between phenotypes observed in the LHCII organization and the thylakoid structure? There are several possibilities. First, RIQ proteins may regulate LHCII organization around PSII to adjust photoprotective functions, such as qE and state transitions. The structural alteration of grana membranes observed in *riq* mutants may have been secondarily affected by the impaired flexibility of LHCIIs. The thylakoid membrane is crowded with proteins, restricting their lateral diffusion (Kirchhoff et al., 2008). Because protein density is especially high in the grana, which are rich in PSII and LHCIIs (Dekker and Boekema, 2005), specific mechanisms may be needed for LHCII reorganization (Kouřil et al., 2012). In plants in which LHCIIs levels are artificially modulated, the degree of grana stacking depends on the LHCIIs level (Labate et al., 2004; Pietrzykowska et al., 2014). However, this idea is unlikely to explain the *riq* phenotype because the LHCII level was unaffected in *riq* mutants (Supplemental Figure 6 and Supplemental Table 1). We detected an even smaller size of antennae, which were functionally connected to the PSII core (Figure 6A). It is also unlikely that the greater stacking of the grana occurred via alteration of the phosphorylation of thylakoid proteins because there was no difference in phosphorylation profile of thylakoid proteins between the wild type and *riq* mutants (Supplemental Figure 8). We cannot eliminate the possibility that the mild alteration in antenna organization around PSII produced unusual free LHCIIs, accelerating the grana stacking.

Alternatively, RIQ proteins may directly regulate the extent of grana stacking and, consequently, the optimization of the

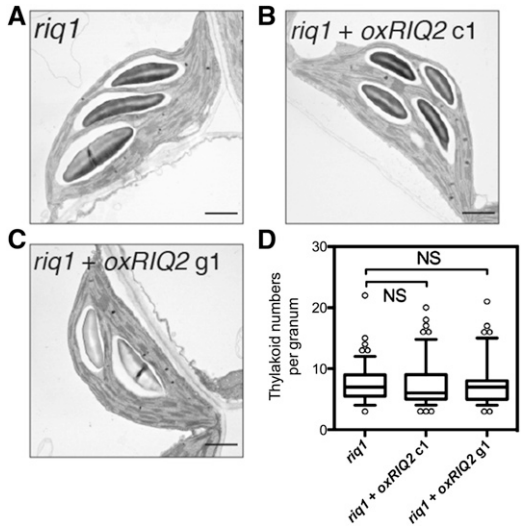

Figure 10. Wild-Type Level of RIQ2 Did Not Complement the Thylakoid Phenotype of *riq1*.

(A) to **(C)** Chloroplast ultrastructures of *riq1* **(A)** and the RIQ2-complemented *riq1* mutants (independent transgenic lines c1 **[B]** and g1 **[C]**), taken from the same samples as shown in Figure 4. Bars = 1 μm.
(D) Quantitative comparison of the number of thylakoid membranes per granum. Grana stacks were randomly chosen from different chloroplasts to count the thylakoid number per granum. For plotting the numbers, boxes extend from the 25th to 75th percentiles. Lines in the middle of the box are plotted at the median. Whiskers are drawn down to the 5th percentile and up to the 95th. Points below and above the whiskers are drawn as individual dots. NS > 0.05, not significant by one-way ANOVA (Dunnett's post hoc test versus *riq1*). *n* (the number of grana stacks measured) = 111 to 121.

LHCII organization. This idea is consistent with the phylogenic distribution of *RIQ* genes in phototrophs developing the grana structure (see below). We cannot eliminate the third possibility that RIQ proteins optimize unknown conditions of the thylakoid membrane that are indirectly and independently required for both normal thylakoid development and LHCII organization.

The *riq* phenotype in NPQ induction is mild and is restricted to low to moderate light. Because NPQ levels rapidly declined to the wild-type level after the AL had been turned off, the partial NPQ relaxation in the light in *riq* mutants likely reflected a defect in qE. NPQ was fully induced in *riq* mutants to wild-type level at 1900 μmol photons m^{-2} s^{-1} (Figure 2B). As proposed for the function of PsbS in NPQ induction (Ruban et al., 2012), RIQ proteins may help increase the sensitivity of LHCIIs to ΔpH by optimizing the grana conditions. When the size of ΔpH is sufficiently large under high light, the function of RIQ proteins may be dispensable.

After a dark adaptation longer than 10 min, *riq* and *curt1a* mutants could induce wild-type levels of NPQ transiently, but this was not the case after a 1-min dark adaptation (Figures 8B and 8C). Our hypothesis is that LHCIIs cannot sustain the state to induce NPQ efficiently under moderate light. This unusual state can be reset after a 10-min dark adaptation, but a 1-min dark interruption was not sufficient. Although reduced activity of the xanthophyll cycle, whose relaxation kinetics in the dark requires several minutes (Nilkens et al., 2010), may cause the phenotype in *curt1a* to some extent, the *riq* phenotype cannot be explained by involvement of the xanthophyll cycle (Supplemental Figure 7). A different cause of reduced NPQ induction was supported by the additive NPQ phenotype of *riq curt1a* mutants.

RIQ proteins are small proteins localized mainly to the grana (Figures 1A and 3C). Although RIQ2 was detected in the fraction of the grana margin and stromal lamella, it may not be due to different localization of RIQ1 and RIQ2, but likely because of higher sensitivity of RIQ2 antibody than RIQ1 antibody, as indicated in the dilution series of Figure 3A. The same localization of RIQ1 and RIQ2 was supported by a previous mass spectrometry study (Tomizioli et al., 2014). Despite the high level of sequence identity between RIQ1 and RIQ2, the functions of the two proteins are not redundant. Phenotypic analyses of the *riq1* mutant accumulating wild-type level of RIQ2 revealed that both RIQ1 and RIQ2 functions are necessary for normal NPQ induction and thylakoid stacking (Figures 4 and 10). Despite the difference in the thylakoid structure, *riq1 curt1a* and *riq2 curt1a* had similar levels of reduction in NPQ (Figure 8A). The NPQ phenotype was not linearly correlated with the phenotype in the thylakoid structure in the *curt1a* background. In *riq1 curt1a*, the abnormal thylakoid structure was explained by the additive effect of the two mutations (Figures 9E and 9F). The *curt1a* mutation made the thylakoid discs larger, whereas the *riq1* mutation caused greater stacking of thylakoids than in *curt1a*, supporting that RIQ and CURT1A proteins contribute to grana formation in different ways.

However, the thylakoid structure phenotype of *riq2 curt1a* suggested that there was a synergistic interaction of the two mutations rather than an additive one (Figures 9G and 9H). Most likely, thylakoid development is more sensitive to the *riq* defect than NPQ induction, and (at least in regard to the function of regulation of the thylakoid structure) RIQ2 cannot solely function in the absence of RIQ1 but likely has an independent or more important function than does RIQ1. We detected some RIQ1 with slightly lower mobility in the gel (Supplemental Figure 3). This specific form of RIQ1 was immunoprecipitated by the anti-RIQ2 antibody (Figure 3D). A modified form of RIQ1 may interact with RIQ2, but further biochemical characterization is needed.

In the Arabidopsis proteome, DUF1118 is specific to RIQ proteins (Figure 1A). The genes encoding proteins with DUF1118 are not found in any photosynthetic prokaryotes, whereas two *RIQ* genes are present in all land plants and some ancient green algae, including *Chlorella*. *Physcomitrella patens* has three isoforms of *RIQ2* orthologs. On the other hand, *Micromonas* does not have a *RIQ2* ortholog, and *Chlamydomonas* and *Volvox* have neither a *RIQ1* nor a *RIQ2* ortholog. In the phylogenetic tree, *RIQ* genes are divided into two clusters, *RIQ1* and *RIQ2* (Figure 1B). This fact suggests that two *RIQ* genes originated from gene duplication in an ancient eukaryotic green phototroph. The genes have been lost during the evolution of green algae. Notably, grana stacking is well developed in land plants (Mullineaux, 2005), in which *RIQ* genes are highly conserved. We propose that *RIQ* genes have conserved roles in land plants to optimize the efficiency of light harvesting and to determine grana structure, which might play an advantageous role in survival under the severe growth conditions on land.

METHODS

Plant Materials and Growth Conditions

Arabidopsis thaliana wild type (Columbia *gl1*) and mutants were grown in a growth chamber under fluorescent light (50 μmol photons m^{-2} s^{-1}, 16-h-light/8-h-dark cycles, 23°C) for ~4 weeks. Plants used in the ECS analysis were cultured under short-day conditions (8-h-light/16-h-dark cycles) for ~8 weeks. *riq1* (SALK_048774), *riq2* (SK6062), and *curt1a* (SK24234) were obtained from the Arabidopsis Biological Resource Center and backcrossed three times with the wild type. *npq4*, *stn7* (SALK_073254), and *ch1-1* were kindly provided by Krishna K. Niyogi (University of California, Berkeley), Masakazu Iwai (University of California, Berkeley), and Ayumu Tanaka (Hokkaido University), respectively.

RNA Isolation and RT-PCR Analysis

Total RNA was prepared from rosette leaves using an RNeasy plant mini kit (Qiagen). Contaminating DNA was digested with DNase I. Total RNA was reverse-transcribed with random hexamers using a PrimeScript first-strand cDNA synthesis kit (TaKaRa Bio). cDNA was used in subsequent PCR with TaKaRa Ex Taq DNA polymerase (TaKaRa Bio) and specific primers listed in Supplemental Table 2. PCRs consisted of 30 s of denaturation at 94°C, 20 s of annealing at 55°C, and a 1-min extension at 72°C. RT-PCR products were separated on a 1.0% agarose gel and detected by ethidium bromide staining.

Chlorophyll Fluorescence and ECS Analyses

For the analyses, three to five individual leaves were chosen from different plants. Chlorophyll fluorescence was measured with a MINI-PAM portable chlorophyll fluorometer (Walz). Minimum fluorescence from open PSII centers in the dark-adapted state (Fo) was excited by a weak measuring light (wavelength 650 nm) at a light intensity of 0.05 to 0.1 μmol photons m^{-2} s^{-1}. A saturating pulse of white light (800 ms, 3000 μmol photons m^{-2} s^{-1}) was applied to determine the maximum fluorescence from closed PSII reaction centers in the dark-adapted state (Fm) and during white AL illumination (Fm′). The steady state fluorescence level (Fs) was recorded during AL illumination (20 to 1000 μmol photons m^{-2} s^{-1}). NPQ was calculated as (Fm–Fm′)/Fm′. For the analysis of the light intensity dependence of fluorescence parameters, the intensity of AL was increased in a stepwise manner every 2 min after application of a saturating pulse. To measure NPQ induction under red AL, a DUAL-PAM-100 system (Walz) was used with supply of 635-nm red light. ECS signals were detected as an absorbance change at 515 nm using a DUAL-PAM-100 system equipped with a P515/535 emitter-detector module (Walz), as described previously (Wang et al., 2015). ECS_{ST} was determined as 515-nm absorbance changes using a single turnover flash and used to standardize ECS_t. ECS_t was monitored as the total amplitude of the decay of the ECS signal using a 1-s dark pulse during steady state photosynthesis at 98, 249, or 1707 μmol photons m^{-2} s^{-1}.

77K Chlorophyll Fluorescence Analysis

Before measurement, leaves were exposed to far red light or weak red light (30 μmol photons m^{-2} s^{-1}) for at least 30 min to induce state 1 and state 2, respectively. Fluorescence was measured with a spectrofluorometer (FP-8500; JASCO) equipped with a low temperature unit (PMU-830; JASCO) filled with liquid nitrogen. The excitation wavelength was 435 nm, and the fluorescence emission was monitored from 600 to 800 nm. After curve fitting, the levels were normalized against the peak from PSI to compare the fluorescence intensities of the PSII antennae.

Flash Fluorescence Induction

A saturating flash of 100 μs duration was applied to isolated thylakoids, corresponding to 5 μg chlorophyll/mL, in the presence of 10 μM DCMU. The chlorophyll fluorescence induction was recorded with a dual-modulation fluorometer (FL 3500/F; Photon Systems Instruments).

Carotenoid Analysis

After dark adaptation, three leaves detached from different plants were placed on a wet paper and exposed to white light (250 μmol photons m^{-2} s^{-1}) for 5 min and then immersed immediately in liquid nitrogen. The frozen leaves were ground in a mortar and solubilized with 1 mL 85% (v/v) acetone. The samples were centrifuged at 1110*g* for 10 min. The pellet was resuspended for repeated washing with 1 mL 100% acetone until the supernatants and the pellets became completely colorless. After 100% acetone was added to the extracts obtained (up to 3 mL), each sample was filtered through a 0.2-μm filter and then applied to HPLC with a column (YMC-Pack ODS-AL AL12S05) designed for the detection of carotenoids by UV-970 (JASCO). From pigment extraction to sample application to HPLC, experiments were performed under as dark and cold conditions as possible.

Transformation of Plants

For complementation of *riq* mutants, Arabidopsis genomic sequences amplified by PCR were cloned into the pDONR/Zeo (Life Technologies) vector using the BP clonase reaction (Life Technologies) and then transferred to the binary vector pGWB-NB1 (Nakagawa et al., 2007) using the LR clonase reaction (Life Technologies). For expression of *RIQ2* under the control of the CaMV 35S promoter, the Arabidopsis cDNA sequence amplified by PCR was cloned into the pDONR/Zeo (Life Technologies) vector using the BP clonase reaction (Life Technologies), followed by transfer to the binary vector pGWB2 (Nakagawa et al., 2007) by LR clonase reaction (Life Technologies). For complementation of *curt1a*, cDNA amplified by PCR was cloned into the pENTR/D-TOPO (Life Technologies) vector using the TOPO cloning method (Life Technologies). This was followed by insertion of the hemagglutinin tag sequence (YPYDVPDYA) by PCR. This entry vector was then transferred to the binary vector pGWB2 (Nakagawa et al., 2007) using the LR clonase reaction (Life Technologies). The resultant vectors were transformed into *Agrobacterium tumefaciens* C58C by electroporation, and these bacteria were used to transform the *riq1* or *curt1a* plants using a modified floral dip method (Martinez-Trujillo et al., 2004). Transformed plants were selected on media containing kanamycin and hygromycin for both pGWB vectors. Homozygous transformants in the T3 generation were used for the analyses.

Production of Antisera against RIQ1, RIQ2, and CURT1A

For production of the antibodies that recognize predicted mature forms of RIQ proteins, cDNAs encoding the mature sequences of RIQ1 (amino acids 41 to 158) and RIQ2 (45 to 198) were amplified by PCR for cloning into pENTR-D-TOPO using a TOPO PCR cloning kit (Life Technologies). In order to express His-tagged recombinant proteins, cDNAs were digested with *Bfa*I and *Bam*HI for *RIQ1* and *Nde*I and *Bam*HI for *RIQ2*, and cloned into pET22b (Novagen) and pET16b (Novagen), respectively. *Escherichia coli* Rosetta (DE3) pLysS cells (Novagen) transformed with these plasmids were used for expression of the recombinant proteins. Expression was induced by treatment with 1 mM isopropyl β-D-thiogalactopyranoside for 12 h at 37°C. Cells were collected by centrifugation at 4612*g* for 10 min and disrupted by sonication on ice in 25 mL of binding buffer (20 mM sodium phosphate buffer, pH 7.4, containing 30 mM imidazole and 500 mM NaCl). The inclusion bodies were pelleted by centrifugation at 2952*g* for 20 min, washed with binding buffer three times, and then sonicated in 30 mL of solubilization buffer (binding buffer containing 6 M urea). Insoluble proteins were removed by centrifugation at 33,200*g* for 2 h. The supernatant was filtered through a 0.4-μm filter and incubated with 2 mL Ni^{2+}-NTA Agarose (Qiagen) for 3 h at 4°C. After washing the agarose three times with 25 mL of

solubilization buffer, bound His-tagged fusion proteins were eluted with 4 mL of elution buffer (solubilization buffer containing 500 mM imidazole). Polyclonal antisera were raised in rabbits using the purified proteins. A rabbit polyclonal anti-CURT1A antibody was prepared against the ASSEETSSIDTNELITDLKEKWDGLENK sequence conjugated with keyhole limpet hemocyanin (Eurofins Genomics). An anti-RIQ1 antibody was prepared against the EEFGVLSAATNPET sequence in a similar manner.

Chloroplast and Thylakoid Preparation

Leaves of 4- to 5-week-old plants were homogenized in a buffer containing 330 mM sorbitol, 20 mM HEPES-KOH (pH 7.6), 5 mM $MgCl_2$, and 2.5 mM EDTA. Chloroplasts were precipitated by centrifugation at 15,000*g* for 5 min and resuspended in 300 mM sorbitol, 20 mM HEPES/KOH (pH 7.6), 5 mM $MgCl_2$, and 2.5 mM EDTA. Freshly isolated chloroplasts were osmotically ruptured in a buffer containing 20 mM HEPES/KOH (pH 7.6), 5 mM $MgCl_2$, and 2.5 mM EDTA and then precipitated by centrifugation at 15,000*g* for 5 min (insoluble fraction). The concentration of chlorophyll was determined with a spectrophotometer and 80%-acetone-suspended thylakoids, as described by Porra et al. (1989). Finally, a sample buffer (50 mM Tris-HCl, pH 6.8, 2% SDS, 10% glycerol, 1% β-mercaptoethanol, and 0.1% bromophenol blue) was added for further SDS-PAGE analysis. For subfractionation of grana stacks, grana margins, and stromal lamellae, intact chloroplasts were ruptured in 200 mL of Tricine 10 buffer (10 mM Tricine, 10 mM NaCl, and 10 mM $MgCl_2$, pH 7.8) and incubated on ice for 10 min. After the determination of chlorophyll concentration, the membrane fraction was pelleted by centrifugation at 15,000*g* for 5 min and then resuspended at 1.5 mg chlorophyll/mL in Tricine 100 buffer (Tricine 10 buffer containing 100 mM Tricine) at room temperature. Digitonin dissolved in the same volume of Tricine 100 buffer as the thylakoids at a digitonin to chlorophyll ratio of ~11 (w/w) was added and the mixture was then incubated for 3 min at room temperature. After centrifugation of the mixture at 1000*g* for 2 min, the supernatant was centrifuged at 10,000*g* for 30 min to obtain the grana core. The grana margin was pelleted from this supernatant at 20,000*g* for 20 min. The supernatant was then ultracentrifuged at 150,000*g* for 1 h. The final pelleted fraction represented stromal lamella proteins. To separate membrane fractions of chloroplasts, intact chloroplasts were frozen at –20°C and thawed at room temperature twice in a buffer containing 0.6 M sucrose, 10 mM Tricine (pH 7.5), and 2 mM EDTA. Envelopes and thylakoid membranes were then separated using a 0.3 to 1.3 M sucrose gradient by ultracentrifugation at 118,000*g* for 16 h. Chloroplasts were also osmotically ruptured in a buffer containing 20 mM HEPES-KOH (pH 7.6), 5 mM $MgCl_2$, and 2.5 mM EDTA and then centrifuged at 15,000*g* for 5 min to obtain the supernatant, which was used as the soluble stromal fraction. All operations were performed at 4°C.

SDS-PAGE and Immunoblot Analysis

SDS-PAGE and immunoblot analysis were performed as shown previously (Yamamoto et al., 2011). For immunodetection of phosphorylated thylakoid proteins, each state was induced in leaves as described in 77K chlorophyll fluorescence analysis. Thylakoid proteins were immediately isolated and then analyzed as described with some modifications. All the buffers used during the isolation process contained 10 mM NaF to inhibit unintended phosphorylation. Major phosphorylated thylakoid proteins were detected using an antiphosphothreonine antibody (New England Biolabs).

Coimmunoprecipitation

For immunoprecipitation, magnetic beads corresponding to 50 μL Dynabeads Protein A for Immunoprecipitation (Life Technologies) were resuspended with 10 μL polyclonal antibody and 190 μL sodium phosphate buffer (20 mM, pH 7.0). They were incubated for 2 h and then washed with 900 μL of the same buffer. Isolated thylakoids corresponding to 100 μg chlorophyll were solubilized with 200 μL of the isolation buffer (20 mM HEPES/KOH, pH 7.6, 5 mM $MgCl_2$, and 2.5 mM EDTA) plus 1.0% (v/v) β-dodecylmaltoside for 10 min. After centrifugation of the mixture at 12,000*g* for 10 min, the supernatants were incubated with the beads for 3 h and washed five times with 900 μL of isolation buffer supplemented with 350 mM NaCl. Immunoprecipitated proteins were eluted in SDS sample buffer at 70°C for 10 min for further analysis by immunodetection. All operations were performed at 4°C.

Transmission Electron Microscopy Observation

After 3 h of exposure to growth light, 4-week-old leaves were fixed overnight in 4% paraformaldehyde and 1% glutaraldehyde and then postfixed with 1% osmium tetroxide in 50 mM cacodylate buffer for 2 h at room temperature. The samples were dehydrated with an ethanol series (50 to 100%), which was then replaced with propylene oxide. This was followed by infiltration with propylene oxide and Epon (Epon 812 resin; TAAB Laboratories Equipment) solution (propylene oxide, Epon resin, 1:1 [v/v]) overnight. The samples were subsequently embedded in Epon resin, which was allowed to polymerize at 60°C for 72 h. Ultrathin sections were cut using an ultramicrotome (Leica Ultracut UCT) and mounted on a nickel grid. The sections were stained with 4% uranyl acetate and lead citrate, and observed using a transmitted electron microscopy (Hitachi H-7600).

Bioinformatic Analysis

Protein sequences predicted from Arabidopsis *RIQ* genes and their orthologs were aligned using the ClustalX program (Larkin et al., 2007). A phylogenetic tree was constructed using MrBayes 3.2 (Ronquist and Huelsenbeck, 2003) and drawn by FigTree 1.4.0. Transit peptides and transmembrane domains were predicted using TargetP1.1 (Emanuelsson et al., 2000) and SOSUI 1.11 (Hirokawa et al., 1998), respectively.

Accession Numbers

Sequence data from this article can be found in the Arabidopsis Genome Initiative or GenBank/EMBL databases under the following accession numbers: Ath (*Arabidopsis thaliana*) RIQ1 (AT5G08050), Aly (*Arabidopsis lyrata*) RIQ1 (XP_002871303.1), Osa (*Oryza sativa*) RIQ1 (NP_001067105.1, Os12g38640), Zma (*Zea mays*) RIQ1 (NP_001141309.1), Ppa (*Physcomitrella patens*) RIQ1 (XP_001760592.1), Cva (*Chlorella variabilis*) RIQ1 (XP_005847850.1), Mpu (*Micromonas pusilla RCC299*) RIQ1 (XP_002503788.1), At RIQ2 (AT1G74730), Aly RIQ2 (XP_002887556.1), Osa RIQ2 (NP_001043425.1, Os01g0585300), Zma RIQ2 (NP_001143840.1), Ppa RIQ2a (XP_001762802.1), Ppa RIQ2b (XP_001778555.1), Ppa RIQ2c (XP_001779946.1), Cva RIQ2 (XP_005852068.1), and Ath CURT1A (AT4G01150).

Supplemental Data

Supplemental Figure 1. The NPQ Phenotype in *riq* Mutants Was Complemented by Introduction of *RIQ* Genes.

Supplemental Figure 2. Reduced NPQ Was Observed in *riq* Mutants under Red Light.

Supplemental Figure 3. Similar Signals of RIQ1 Were Detected Using Two Types of Antibodies.

Supplemental Figure 4. Linear Electron Transport Activity Was Similar in the Wild Type and *riq* Mutants.

Supplemental Figure 5. Proton Motive Force Was Normally Formed in *riq* Mutants.

Supplemental Figure 6. Accumulation of Major Thylakoid Membrane Proteins Was Unaffected in *riq* Mutants.

Supplemental Figure 7. Xanthophyll Cycle Was Normally Operated in *riq* Mutants.

Supplemental Figure 8. Phosphorylation Profile of PSII-Related Proteins Was not Affected in *riq* Mutants.

Supplemental Figure 9. Additional Electron Micrographs of Chloroplasts of the Wild Type and *riq* Mutants.

Supplemental Figure 10. A Novel Allele of *curt1a* Mutant.

Supplemental Figure 11. Additional Electron Micrographs of Chloroplasts of the Wild Type and *riq* and *curt1a* Mutants.

Supplemental Table 1. Chlorophyll Content and Chlorophyll *a*/*b* Ratio.

Supplemental Table 2. List of Primers Used in This Study.

Supplemental Data Set 1. Sequences and Alignment Used for the Phylogenetic Analysis Shown in Figure 1B.

ACKNOWLEDGMENTS

R.Y. was financially supported as a research fellow of the Japan Society for the Promotion of Science. T.S. was supported by the Japanese Society for the Promotion of Science (25251032). This work was supported by an NIBB Collaborative Research Program grant (14-378) to T.S. We thank Tsuyoshi Nakagawa (Shimane University) and Amane Makino (Tohoku University) for providing the pGWB vectors and Cyt *f* antibody, respectively.

AUTHOR CONTRIBUTIONS

R.Y., Y.H., and T.S. designed the experiments. R.Y. mainly performed the experiments. Y.F. performed the proteome analysis. M.K., Y.K., and M.N. performed the transmission electron microscopy analysis. K.I. helped with the analyses of LHCII organization. S.T. performed the HPLC analysis. R.Y. and T.S. wrote the article.

Received April 14, 2016; revised August 1, 2016; accepted September 3, 2016; published September 6, 2016.

REFERENCES

Armbruster, U., et al. (2013). *Arabidopsis* CURVATURE THYLAKOID1 proteins modify thylakoid architecture by inducing membrane curvature. Plant Cell **25:** 2661–2678.

Aro, E.M., Virgin, I., and Andersson, B. (1993). Photoinhibition of photosystem II. Inactivation, protein damage and turnover. Biochim. Biophys. Acta **1143:** 113–134.

Bellafiore, S., Barneche, F., Peltier, G., and Rochaix, J.D. (2005). State transitions and light adaptation require chloroplast thylakoid protein kinase STN7. Nature **433:** 892–895.

Cazzaniga, S., Dall' Osto, L., Kong, S.G., Wada, M., and Bassi, R. (2013). Interaction between avoidance of photon absorption, excess energy dissipation and zeaxanthin synthesis against photooxidative stress in Arabidopsis. Plant J. **76:** 568–579.

Cui, Y.L., Jia, Q.S., Yin, Q.Q., Lin, G.N., Kong, M.M., and Yang, Z.N. (2011). The *GDC1* gene encodes a novel ankyrin domain-containing protein that is essential for grana formation in *Arabidopsis.* Plant Physiol. **155:** 130–141.

de Bianchi, S., Betterle, N., Kouril, R., Cazzaniga, S., Boekema, E., Bassi, R., and Dall'Osto, L. (2011). *Arabidopsis* mutants deleted in the light-harvesting protein Lhcb4 have a disrupted photosystem II macrostructure and are defective in photoprotection. Plant Cell **23:** 2659–2679.

de Bianchi, S., Dall'Osto, L., Tognon, G., Morosinotto, T., and Bassi, R. (2008). Minor antenna proteins CP24 and CP26 affect the interactions between photosystem II subunits and the electron transport rate in grana membranes of *Arabidopsis.* Plant Cell **20:** 1012–1028.

Dekker, J.P., and Boekema, E.J. (2005). Supramolecular organization of thylakoid membrane proteins in green plants. Biochim. Biophys. Acta **1706:** 12–39.

Emanuelsson, O., Nielsen, H., Brunak, S., and von Heijne, G. (2000). Predicting subcellular localization of proteins based on their N-terminal amino acid sequence. J. Mol. Biol. **300:** 1005–1016.

Espineda, C.E., Linford, A.S., Devine, D., and Brusslan, J.A. (1999). The *AtCAO* gene, encoding chlorophyll *a* oxygenase, is required for chlorophyll *b* synthesis in *Arabidopsis thaliana.* Proc. Natl. Acad. Sci. USA **96:** 10507–10511.

Fleischmann, M.M., Ravanel, S., Delosme, R., Olive, J., Zito, F., Wollman, F.A., and Rochaix, J.D. (1999). Isolation and characterization of photoautotrophic mutants of *Chlamydomonas reinhardtii* deficient in state transition. J. Biol. Chem. **274:** 30987–30994.

Fristedt, R., Willig, A., Granath, P., Crèvecoeur, M., Rochaix, J.D., and Vener, A.V. (2009). Phosphorylation of photosystem II controls functional macroscopic folding of photosynthetic membranes in *Arabidopsis.* Plant Cell **21:** 3950–3964.

Havaux, M., Dall'osto, L., and Bassi, R. (2007). Zeaxanthin has enhanced antioxidant capacity with respect to all other xanthophylls in Arabidopsis leaves and functions independent of binding to PSII antennae. Plant Physiol. **145:** 1506–1520.

Hirokawa, T., Boon-Chieng, S., and Mitaku, S. (1998). SOSUI: classification and secondary structure prediction system for membrane proteins. Bioinformatics **14:** 378–379.

Holzwarth, A.R., Miloslavina, Y., Nilkens, M., and Jahns, P. (2009). Identification of two quenching sites active in the regulation of photosynthetic light-harvesting studied by time-resolved fluorescence. Chem. Phys. Lett. **483:** 262–267.

Horton, P., Ruban, A.V., and Walters, R.G. (1996). Regulation of light harvesting in green plants. Annu. Rev. Plant Physiol. Plant Mol. Biol. **47:** 655–684.

Jahns, P., and Holzwarth, A.R. (2012). The role of the xanthophyll cycle and of lutein in photoprotection of photosystem II. Biochim. Biophys. Acta **1817:** 182–193.

Johnson, M.P., Goral, T.K., Duffy, C.D., Brain, A.P., Mullineaux, C.W., and Ruban, A.V. (2011). Photoprotective energy dissipation involves the reorganization of photosystem II light-harvesting complexes in the grana membranes of spinach chloroplasts. Plant Cell **23:** 1468–1479.

Kim, E.H., Li, X.P., Razeghifard, R., Anderson, J.M., Niyogi, K.K., Pogson, B.J., and Chow, W.S. (2009). The multiple roles of light-harvesting chlorophyll *a*/*b*-protein complexes define structure and optimize function of *Arabidopsis* chloroplasts: a study using two chlorophyll *b*-less mutants. Biochim. Biophys. Acta **1787:** 973–984.

Kirchhoff, H., Haferkamp, S., Allen, J.F., Epstein, D.B., and Mullineaux, C.W. (2008). Protein diffusion and macromolecular crowding in thylakoid membranes. Plant Physiol. **146:** 1571–1578.

Kouřil, R., Dekker, J.P., and Boekema, E.J. (2012). Supramolecular organization of photosystem II in green plants. Biochim. Biophys. Acta **1817:** 2–12.

Labate, M.T., Ko, K., Ko, Z.W., Pinto, L.S., Real, M.J., Romano, M.R., Barja, P.R., Granell, A., Friso, G., van Wijk, K.J., Brugnoli, E., and Labate, C.A. (2004). Constitutive expression of pea Lhcb 1-2 in tobacco affects plant development, morphology and photosynthetic capacity. Plant Mol. Biol. **55:** 701–714.

Larkin, M.A., et al. (2007). Clustal W and Clustal X version 2.0. Bioinformatics **23:** 2947–2948.

Li, X.P., Björkman, O., Shih, C., Grossman, A.R., Rosenquist, M., Jansson, S., and Niyogi, K.K. (2000). A pigment-binding protein essential for regulation of photosynthetic light harvesting. Nature **403:** 391–395.

Li, Z., Wakao, S., Fischer, B.B., and Niyogi, K.K. (2009). Sensing and responding to excess light. Annu. Rev. Plant Biol. **60:** 239–260.

Martinez-Trujillo, M., Limones-Briones, V., Cabrera-Ponce, J.L., and Herrera-Estrella, L. (2004). Improving transformation efficiency of *Arabidopsis* thaliana by modifying the floral dip method. Plant Mol. Biol. Report. **22:** 63–70.

Minagawa, J. (2013). Dynamic reorganization of photosynthetic supercomplexes during environmental acclimation of photosynthesis. Front. Plant Sci. **4:** 513.

Mullineaux, C.W. (2005). Function and evolution of grana. Trends Plant Sci. **10:** 521–525.

Murray, D.L., and Kohorn, B.D. (1991). Chloroplasts of *Arabidopsis thaliana* homozygous for the *ch-1* locus lack chlorophyll *b*, lack stable LHCPII and have stacked thylakoids. Plant Mol. Biol. **16:** 71–79.

Nakagawa, T., Kurose, T., Hino, T., Tanaka, K., Kawamukai, M., Niwa, Y., Toyooka, K., Matsuoka, K., Jinbo, T., and Kimura, T. (2007). Development of series of gateway binary vectors, pGWBs, for realizing efficient construction of fusion genes for plant transformation. J. Biosci. Bioeng. **104:** 34–41.

Nedbal, L., Trtilek, M., and Kaftan, D. (1999). Flash fluorescence induction: a novel method to study regulation of photosystem II. J. Photochem. Photobiol. **48:** 154–157.

Nilkens, M., Kress, E., Lambrev, P., Miloslavina, Y., Müller, M., Holzwarth, A.R., and Jahns, P. (2010). Identification of a slowly inducible zeaxanthin-dependent component of non-photochemical quenching of chlorophyll fluorescence generated under steady-state conditions in *Arabidopsis.* Biochim. Biophys. Acta **1797:** 466–475.

Niyogi, K.K., Grossman, A.R., and Björkman, O. (1998). *Arabidopsis* mutants define a central role for the xanthophyll cycle in the regulation of photosynthetic energy conversion. Plant Cell **10:** 1121–1134.

Pietrzykowska, M., Suorsa, M., Semchonok, D.A., Tikkanen, M., Boekema, E.J., Aro, E.M., and Jansson, S. (2014). The light-harvesting chlorophyll *a*/*b* binding proteins Lhcb1 and Lhcb2 play complementary roles during state transitions in *Arabidopsis.* Plant Cell **26:** 3646–3660.

Porra, R.J., Thompson, W.A., and Kriedemann, P.E. (1989). Determination of accurate extinction coefficients and simultaneous equations for assaying chlorophylls *a* and *b* extracted with four different solvents: verification of the concentration of chlorophylls standards by atomic absorption spectroscopy. Biochim. Biophys. Acta **975:** 384–394.

Pribil, M., Labs, M., and Leister, D. (2014). Structure and dynamics of thylakoids in land plants. J. Exp. Bot. **65:** 1955–1972.

Puthiyaveetil, S., Tsabari, O., Lowry, T., Lenhert, S., Lewis, R.R., Reich, Z., and Kirchhoff, H. (2014). Compartmentalization of the protein repair machinery in photosynthetic membranes. Proc. Natl. Acad. Sci. USA **111:** 15839–15844.

Ronquist, F., and Huelsenbeck, J.P. (2003). MrBayes 3: Bayesian phylogenetic inference under mixed models. Bioinformatics **19:** 1572–1574.

Ruban, A.V., Johnson, M.P., and Duffy, C.D. (2012). The photoprotective molecular switch in the photosystem II antenna. Biochim. Biophys. Acta **1817:** 167–181.

Standfuss, J., Terwisscha van Scheltinga, A.C., Lamborghini, M., and Kühlbrandt, W. (2005). Mechanisms of photoprotection and nonphotochemical quenching in pea light-harvesting complex at 2.5 A resolution. EMBO J. **24:** 919–928.

Sun, Q., Zybailov, B., Majeran, W., Friso, G., Olinares, P.D.B., and van Wijk, K.J. (2009). PPDB, the plant proteomics database at Cornell. Nucleic Acids Res. **37:** D969–D974.

Takabayashi, A., Kurihara, K., Kuwano, M., Kasahara, Y., Tanaka, R., and Tanaka, A. (2011). The oligomeric states of the photosystems and the light-harvesting complexes in the Chl *b*-less mutant. Plant Cell Physiol. **52:** 2103–2114.

Tomizioli, M., et al. (2014). Deciphering thylakoid sub-compartments using a mass spectrometry-based approach. Mol. Cell. Proteomics **13:** 2147–2167.

Wang, C., Yamamoto, H., and Shikanai, T. (2015). Role of cyclic electron transport around photosystem I in regulating proton motive force. Biochim. Biophys. Acta **1847:** 931–938.

Yamamoto, H., Peng, L., Fukao, Y., and Shikanai, T. (2011). An Src homology 3 domain-like fold protein forms a ferredoxin binding site for the chloroplast NADH dehydrogenase-like complex in Arabidopsis. Plant Cell **23:** 1480–1493.